



THE UNIVERSITY *of* EDINBURGH

Edinburgh Research Explorer

Relationships of S-Band Radar Backscatter and Forest Aboveground Biomass in Different Forest Types

Citation for published version:

Ningthoujam, RK, Balzter, H, Tansey, K, Feldpausch, TR, Mitchard, E, Wani, AA & Joshi, PK 2017, 'Relationships of S-Band Radar Backscatter and Forest Aboveground Biomass in Different Forest Types' Remote Sensing. DOI: 10.3390/rs9111116

Digital Object Identifier (DOI):

[10.3390/rs9111116](https://doi.org/10.3390/rs9111116)

Link:

[Link to publication record in Edinburgh Research Explorer](#)

Document Version:

Publisher's PDF, also known as Version of record

Published In:

Remote Sensing

General rights

Copyright for the publications made accessible via the Edinburgh Research Explorer is retained by the author(s) and / or other copyright owners and it is a condition of accessing these publications that users recognise and abide by the legal requirements associated with these rights.





Take down policy

The University of Edinburgh has made every reasonable effort to ensure that Edinburgh Research Explorer content complies with UK legislation. If you believe that the public display of this file breaches copyright please contact openaccess@ed.ac.uk providing details, and we will remove access to the work immediately and investigate your claim.



Article

Relationships of S-Band Radar Backscatter and Forest Aboveground Biomass in Different Forest Types

Ramesh K. Ningthoujam ^{1,2,*} , Heiko Balzter ^{1,3,†} , Kevin Tansey ^{1,†}, Ted R. Feldpausch ⁴ , Edward T. A. Mitchard ⁵ , Akhlaq A. Wani ⁶ and Pawan K. Joshi ⁷

¹ School of Geography, Geology and the Environment, Centre for Landscape and Climate Research, University of Leicester, Leicester LE1 7RH, UK; hb91@le.ac.uk (H.B.); kjt7@le.ac.uk (K.T.)

² Department of Life Sciences, Imperial College London, Silwood Park Campus, Buckhurst Road, Ascot SL5 7PY, UK

³ National Centre for Earth Observation (NCEO), University of Leicester, Leicester LE1 7RH, UK

⁴ Geography, College of Life and Environmental Sciences, University of Exeter, Exeter EX44RJ, UK; T.R.Feldpausch@exeter.ac.uk

⁵ School of Geosciences, University of Edinburgh, Edinburgh EH9 3FF, UK; Edward.Mitchard@ed.ac.uk

⁶ Faculty of Forestry, Sher-e-Kashmir University of Agricultural Sciences and Technology of Kashmir, Benhama Ganderbal J&K 191201, India; akhlaqwani@gmail.com

⁷ School of Environmental Sciences, Jawaharlal Nehru University, New Delhi 110067, India; pkjoshi27@hotmail.com

* Correspondence: rningthoujam@sky.com

† These authors contributed equally to this work.

Received: 21 August 2017; Accepted: 30 October 2017; Published: 2 November 2017

Abstract: Synthetic Aperture Radar (SAR) signals respond to the interactions of microwaves with vegetation canopy scatterers that collectively characterise forest structure. The sensitivity of S-band (7.5–15 cm) backscatter to the different forest types (broadleaved, needleleaved) with varying aboveground biomass (AGB) across temperate (mixed, needleleaved) and tropical (broadleaved, woody savanna, secondary) forests is less well understood. In this study, Michigan Microwave Canopy Scattering (MIMICS-I) radiative transfer model simulations showed strong volume scattering returns from S-band SAR for broadleaved canopies caused by ground/trunk interactions. A general relationship between AirSAR S-band measurements and MIMICS-I simulated radar backscatter with forest AGB up to nearly 100 t/ha in broadleaved forest in the UK was found. Simulated S-band backscatter-biomass relationships suggest increasing backscatter sensitivity to forest biomass with a saturation level close to 100 t/ha and errors between 37 t/ha and 44 t/ha for HV and VV polarisations for tropical ecosystems. In the near future, satellite SAR-derived forest biomass from P-band BIOMASS mission and L-band ALOS-2 PALSAR-2 in combination with S-band UK NovaSAR-S and the joint NASA-ISRO NISAR sensors will provide better quantification of large-scale forest AGB at varying sensitivity levels across primary and secondary forests and woody savannas.

Keywords: forest aboveground biomass; MIMICS-I model; AirSAR S-band SAR; temperate; tropics

1. Introduction

Satellite remote sensing technology has shown promising capabilities for consistent and systematic observations of the dynamics of large-scale forest ecosystems [1]. Electromagnetic radiation in the microwave domain is related to forest properties due to its high sensitivity to canopy structure and moisture content. Forest structure information such as tree density, average stand height and diameter at breast height based on sample plots is necessary [2] to calibrate with microwave backscatter signals and for predictions of forest biophysical parameters such as aboveground biomass (AGB) [3].

Synthetic Aperture Radar (SAR) data is often used to quantify forest properties. For instance, airborne and satellite-based SAR sensors at different radar wavelengths (P-, L-, C-, X-band) have been used for estimating forest properties because of the sensitivity of radar signals to complex forest structure [1,2,4]. The ability of the SAR signal to detect forest canopy components (trunks, branches, leaves and needles) depends on its wavelengths (or frequency), incidence angles and polarisations. SAR polarimetry provides information on the physical scattering mechanisms from a forest target, based on the fundamental physical scattering mechanisms of surface scattering from the ground, double-bounce scattering from ground/trunk interactions and volume scattering from the canopy layer depending on the characteristics (material, size, shape, roughness) and position of the target. The sensitivity of radar backscatter to forest structure also depends on the canopy type (intact to open savanna, homogeneity to complex density) and environmental conditions such as moisture content [5]. The co-polarised channels exhibit a large amount of scattered microwave energy with the strongest return at HH polarisation (horizontal transmit horizontal return) due to double-bounce scattering from the vertical trunk structure perpendicular to the ground surface (except in undulating terrain). In comparison, forest biomass is largely related to the cross-polarised channels (HV—horizontal transmit vertical return) which have comparatively lower returns but generally increase asymptotically to the amount of woody biomass up to a saturation level [6,7].

Amongst the different radar wavelengths, studies focusing on S-band data for forest structure and biomass characterisation have rarely been investigated due to limited data availability. Few published studies have investigated S-band radar responses to agricultural crops and forest canopies to date. For example, S-band SAR from the Russian Almaz-1 satellite has been used for mapping clear-felled mixed forests in Ontario [8]. Multi-temporal Almaz-1 data using mean textural information have also been used to identify clear-felled areas in a boreal conifer forest in northern Sweden [9]. Almaz-1 S-band backscatter has a very narrow dynamic range and similar average backscatter values in different vegetation types [10], including palm and rubber plantations. Furthermore, Rosenqvist [10] questioned whether the effect of high incidence angles ($\sim 50^\circ$) is the main factor responsible for poor results in a Malaysian test site compared to the studies by Olsson, et al. [11] and Brown, et al. [12].

The sensitivity of S-band backscatter to maize crops, using an indoor radar system, was dominantly volume scattering due to the random distribution of the whole plants [13]. The Michigan Microwave Canopy Scattering (MIMICS) model suggests that S-band backscatter is sensitive to the temporal dynamics of the structure of wheat crops [14]. In a controlled indoor experiment, S-band backscatter from young fir arises from the needles and branches, resulting in lower volume scattering due to the conical structure of conifer species [15]. Airborne S-band radar backscatter has been used with polarimetric scattering entropy (H/α) and Pauli's decomposition techniques for mapping agricultural crop canopies [16] and forested [17] areas, and salt marsh habitat mapping using a Random Forest algorithm [18]. The sensitivity of S-band backscatter to forest structure and biophysical parameters has not been fully investigated in any published studies.

The effective exploitation of airborne and space-borne SAR for forestry applications relies on sound theoretical understanding of the relationship between backscatter and forest structure parameters such as volume and/or biomass. However, there is both theoretical [19] and empirical [20] evidence showing that under certain conditions backscatter saturation can occur at lower biomass than expected and sometimes saturation does not occur at all. Saturation may be caused by other factors, such as the ratio of dominant stem radius to wavelength [21,22]. Understanding the relationships between SAR backscatter at varying wavelengths and forest canopy parameters is critically important for deriving forest properties. Details of the physical processes governing the relationships between forest biomass and radar measurements are mostly driven through physical modelling parameterised, by field data from specific forest sites, in particular, managed temperate forests [23].

Several airborne SAR campaigns focusing on P-, L- and C-frequencies have taken place over a wide variety of forest biomes [23–25]. An extensive S-band SAR campaign known as the "AirSAR Campaign" was conducted in the UK in 2010 and 2014 [26]. Using the AirSAR Campaign S-band data, the retrieval

of forest structure and biomass was analysed over the mixed temperate forests of Savernake Forest and Wytham Woods. Estimated forest biomass from VV polarised backscatter shows the best agreement with field plot data while HH shows the weakest relationship. For all the polarisations, higher sensitivity between the predicted forest biomass for 2010 and 2014 is found below 150 t/ha in comparison to higher biomass stands. The main goal of this paper is to explore the sensitivities of S-band backscatter to different forest types and biomass levels. Therefore, further research into the sensitivity of S-band from intact tropical forest to open type forest (savanna) and secondary forest of Amazonia needs to be investigated in preparation for current (Huan Jing-1 Constellation) and future space-borne (NovaSAR-S and NASA ISRO joint NISAR) S-band SAR missions.

In this paper, we provide a detailed analysis of the scattering mechanisms in forest canopies for S-band SAR using the 2014-acquired airborne data and radiative transfer (RT) Michigan Microwave Canopy Scattering model (MIMICS-I), and the validation of the MIMICS-I predictions against the measured data. Applying the knowledge about S-band radar scattering from the temperate forest site, sensitivity to forest biomass utilising simulated S-band backscatter from different forest properties such as intact to open forest and broadleaved to needleleaved types are further investigated.

2. Experimental Section

2.1. Description of Study Sites

Six study sites were chosen to represent vegetation structural diversity between regions (temperate and tropical), the characteristics of the forest (intact, secondary and open forests), no history of recent anthropogenic disturbance and the availability of field data. The variation in biomes and forest structure of our study sites provides a wide range of values to test the potential of radar data for forest biomass assessment. The sites include temperate mixed forest in the UK, tropical primary and secondary forest in Brazil, tropical humid forest in Cameroon and temperate conifer and tropical broadleaved forests in India (Table 1). The UK study sites have been investigated earlier for testing the potential of airborne S-band SAR data in quantification of forest properties. No high-resolution S-band SAR data of Brazilian, Cameroon and India test sites were available to the authors. Only plot-based forest-stand attribute data from these regions was available and this is used to parameterise the MIMICS-I model.

Table 1. Summary of test sites with forest structural characteristics.

Site (Forest Type)	Structural Characteristics
Savernake forest (Temperate Mixed Deciduous, Conifer)	Dominant broadleaved and conifer species have high density wood (30 m tall, 50 cm diameter), closed multi-storey canopy.
Wytham Woods (Temperate Mixed Deciduous)	Mature broadleaved trees are having density wood up to 180 cm diameter and 30 m tall closed, multi-level canopy.
Tapajós (Tropical Primary Ombrophilous Forests of Lowlands, Secondary forest stages-initial, intermediate, advanced)	Mature trees up to 40 m tall, closed, multi-storey canopy. Secondary forests are fast growing up to 15 m tall with more open canopies.
Cameroon (Tropical humid forest-savanna)	Open savanna with 10–30% canopy cover and 10 m tall, up to closed canopy dense forest with tree heights reaching up to 45 m.
Kashmir (Temperate Himalayan dry deciduous-subalpine Fir, alpine scrub, pastures)	Primarily irregular (uneven aged) conifer species attaining a height up to 35 m and 190 cm diameter. Broadleaved species occur sparsely at lower and alpine elevations.
Dudhwa National Park (Tropical Semi-evergreen, Moist deciduous)	Mature broadleaved species have density wood up to 45 m tall, 200 cm diameter with high density multi-storey canopy.

Savernake forest (51°23'13"N, 1°43'19"W) is located near Marlborough in England having an average elevation of 107 m and 1% slope with a south-eastern aspect [27] (Figure 1a). Main deciduous species include *Fagus sylvatica*, *Betula pendula* and *Quercus* spp. while *Pinus sylvestris*, *Pinus nigra* and *Picea abies* are the dominant coniferous species. Wytham Woods (51°47'N, 1°20'W) is situated in the

west of Oxfordshire in south England (Figure 1b). The site represents a mixture of ancient semi-natural woodland with mixed *Fraxinus excelsior*, *Acer campestre* and *Mercurialis perennis* defined in the UK National Vegetation Classification community W8 [28] covering approximately 340 ha.

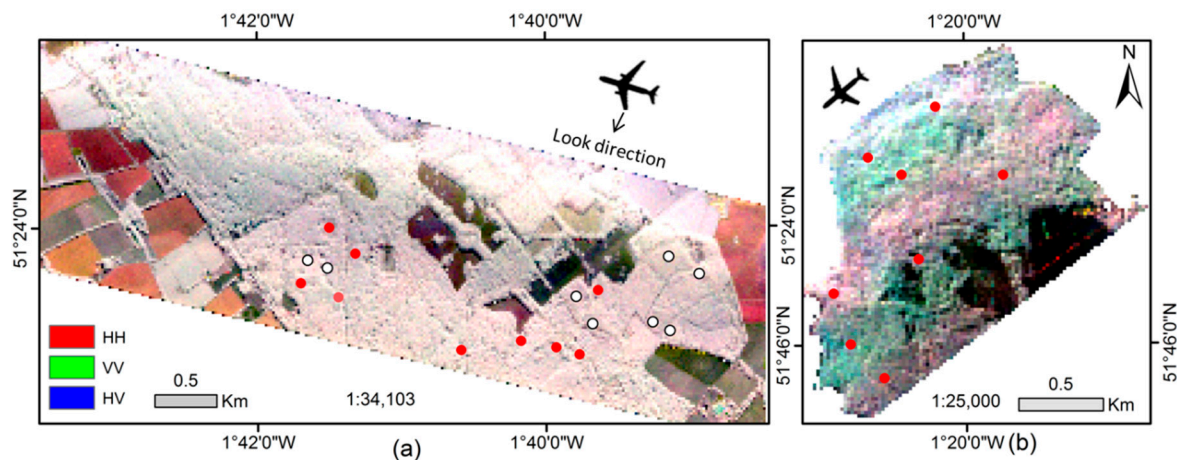


Figure 1. Re-sampled finer resolution (25 m) S-band data acquired over (a) Savernake and (b) Wytham in June 2014 (False colour composite: red: HH, green: VV, blue: HV) with sampled broadleaved stand plots (red dot) and needleleaved stand plots (white with black border dot in Savernake).

The Tapajós site ($54^{\circ}53' - 55^{\circ}06'W$, $3^{\circ}03' - 3^{\circ}12'S$) is in a region of largely intact primary forest and secondary forest, located adjacent to the Tapajós National Forest in the state of Para, Central Brazilian Amazon. According to RADAMBRASIL [29] dominant primary forest species include *Carapa guianensis*, *Syzygiopsis oppositifolia*, *Trattinickia rhoifolia*, *Tachigalia myrmecophylla*, *Coumarou maodorata*, *Nectandra mollis* within dense lowland ombrophilous forests having a large number of emergent individuals and open forests without palms. Dominant species have dense wood and mature trees grow to, e.g., 10–35 m tall and 0.3–1 m diameter, forming a tall, closed, multi-level canopy. Secondary forests have species at different stages (initial, intermediate and advanced) of *Tapirira guianensis*, *Cecropia* spp., *Vismia guianensis*, *Inga alba* and *Murcia bracteata* as, a consequence of cattle and agricultural activities. Dominant secondary forest species are fast growing, having lower wood density and mature trees growing 8–15 m tall and 0.3–0.6 m diameter, forming more open canopies with little vertical stratification. The study area of Cameroon (centred around $6^{\circ}9'N$, $12^{\circ}50'E$) covers a 15,000 km² region, particularly the MbamDjerem National Park and the surrounding area to the north and east. The region has a high species diversity [30]. This region extends across a range of tropical vegetation types from humid forests contiguous with the Congo Basin tropical forest belt in the south to savanna with narrow gallery forests in the north. The main forest species includes *Uapaca guineensis*, *Xylopia aethiopica*, *Maprounea membranacea*, *Berlinia grandiflora* and *Trilepisium madagascariense* where mature trees are on average taller than those of the central Amazonia site [31]. It ranges from open savanna with 10–30% canopy cover and 10 m tall, up to closed canopy dense forest with tree heights reaching up to 45 m.

The temperate coniferous forest of Himalaya ($33^{\circ}21' - 34^{\circ}15'N$, $74^{\circ}52' - 75^{\circ}32'E$) lies in the southern Kashmir. The main forest types include lower Western Himalayan temperate forest, West Himalayan dry temperate deciduous forest, West Himalayan subalpine fir forest, deciduous alpine scrub and alpine pastures [32]. The forests in the region are predominantly coniferous with *Pinus wallichiana*, *Cedrus deodara*, *Abies pindrow*, *Picea smithiana*, *Taxus baccata* and *Juniperus recurva*. Dudhwa National Park (DNP) ($28^{\circ}18' - 28^{\circ}42'N$, $80^{\circ}28' - 80^{\circ}57'E$) is in the Terai region of Uttar Pradesh, India bordering Nepal. The total park area is about 684 km². *Shorea robusta* forest dominates the landscape followed by semi-evergreen forest, moist deciduous forest, *Terminalia tomentosa* forest, *Acacia catechu*-*Dalbergia sissoo* forest, and *Syzigium cumini* forest [32]. Several stands of *Tectona grandis*, *Eucalyptus hybrid*, *Dalbergia sissoo*, *Acacia catechu* and *Lagerstroemia parviflora* plantations are also found.

2.2. Field Data

In August 2012 and March 2015, a total of 15 circular plots, each of 20 m diameter were established from Savernake Forest while data from 8 square plots of 10 × 10 m from Wytham Woods was collected corresponding to 17 broadleaved and 8 needleleaved forest stands [26,33]. The measurements include trunk diameters, tree height using a measuring tape and a Laser Vertex Hypsometer, and species identification. In September 2000, data from 6 rectangular plots of 10 × 250 m of mature forest and 12 rectangular plots of 10 × 100 m of secondary succession from the Tapajós site was collected. Within each transect, diameter at breast height (>5 cm) and total height were measured using measuring tapes. A field campaign was carried out to collect data from 24 field plots in October–December 2007 in humid forest in Cameroon [30]. This includes 12 one-hectare plots each from savanna and forest sites. Within each transect, diameter at breast height (>10 cm) and total height at species level were measured using tapes and a Laser Vertex Hypsometer.

Furthermore, data from a total of 39 square plots, each of 32 × 32 m was collected from Kashmir in June to October 2010, 2011 and 2013 [34]. Within each plot, species were identified where diameter at breast height (>10 cm) and total height were measured using tree calipers and Ravi's multimeter. In June 2006, data from a total of 28 square plots, each of 20 × 20 m was collected from Dudhwa National Park [35]. Within each plot, diameter at breast height (>10 cm) and total height, at species level were measured using tree calipers and a Spiegel Relaskop. Details of the field data are given in Table 2.

Table 2. Details of field measured forest properties (averages) used in this study.

Site (Plots)	Average CH (m)	Average DBH (cm)	Stand Density (trees/ha)	AGB (t/ha)	Allometric Equations
SF-WW (25)	6–23	7–42	20–350	31–520	[36]
Tapajós (24)	7–13.2	6.5–15.85	141–305	8–271.82	[37,38]
Cameroon (24)	6.6–14.6	11.7–24.6	42–641	6–456	[39]
Kashmir (39)	8–29	13–120	40–1800	29.5–136	[40]
DNP (28)	10–27	15–45	88–220	40–453	[40]

SF—Savernake Forest, WW—Wytham woods, DNP—Dudhwa National Park, CH—Canopy Height, DBH—Diameter at Breast Height, AGB—Aboveground biomass.

2.3. MIMICS-I Modelling

Simulations from RT models provide insights into the detail interactions of microwaves with different components of the canopy as a function of wavelength, incidence angle and polarization [23,41]. In contrast to X-, C-, L- and P-band, the nature of S-band microwave scattering mechanisms in forest canopies is poorly studied due to the historic lack of availability of S-band SAR data. MIMICS-I [41]—a generic canopy structure driven forest canopy-based model designed to simulate radar backscatter based on canopy structure and first-order RT equations was used. The model uses Foldy's method to estimate a mean field as a function of height within the canopy followed by scattering from each canopy components. A forest stand is modelled as two independent horizontal layers as crown and trunk layers over a ground surface. The crown layer consists of flat rectangular discs shaped leaves for broadleaved while needles (conifer species) and branches are modelled as cylinders. The trunk layer is composed of modelled cylinders to represent vertical tree trunks. The ground is modelled as a rough surface described by the root mean square height and correlation length. All the scattering components are characterised by the statistics of their size, position, orientation, density and dielectric. In this study, the sensitivity of S-band SAR frequency to forest canopy and its components is investigated as a function of forest canopy types and biomass density in varying SAR system parameters (multiple polarisations, incidence angles between 15° and 45°).

The MIMICS model has been utilised in a number of studies related to the interpretation of the backscatter interactions with vegetation/forest properties. For example, Bosisio, A.V. et al. [42] assessed the sensitivity of C- and L-band backscatter over oak and pine species using MIMICS and the model developed by Karam et al. [43] across seasonal variations (summer against winter) in Fontainebleau forest, France. In the forest ecosystem of Queensland in Australia, the simulated backscatter using both MIMICS and multi-MIMICS was compared against the AIRSAR data [44]. In the Brazilian Amazon, MIMICS model simulations show good discrimination of primary forest against regeneration stages and soil at longer L-band due to strong volume scattering [45].

Radar canopy backscatter is the overall scattering return back to sensor (receiver) influenced by attenuation from the forest canopy in a pixel resolution cell. In MIMICS-I, the first-order solution contains seven scattering mechanisms related to wave energy propagating through the canopy reaching the ground, reflected and backscattered from the ground surface and returned back through the canopy. The MIMICS-I model has been used to simulate backscatter across frequencies and polarisations in different forest environments, for example, by [26,41,42,44,45]. In this study, field data were obtained from published sources. Details of plot information for Savernake-UK, Tapajós-Brazil and Cameroon-Africa forests are given by references [6,7,26]. Data from Kashmir and Dudhwa National Park, India, are unpublished. The available field measurements from all the sites were used to parameterise the MIMICS-I model prior to simulation.

A full description of the MIMICS-I parameterisation for this study is given in Ningthoujam et al. [26] and references therein. Table 3 describes the different parameters that were used in the MIMICS-I simulation for 17 broadleaved and 8 needleleaved stands at the UK test site. The different parameters used for MIMICS-I simulation for other test sites are given in Appendix A. The parameters describing the trunk layer in the model initialisation were the easiest to collect. For both forest stands, trunk diameter was measured with a tape measure at breast height (dbh), while tree height was measured by means of a Laser Vertex Hypsometer over a population of approximately 10 samples in each stand. The crown thickness was estimated as the measured tree height less the measured height of the first branch. Canopy parameters such as number of leaves/needles/branches, Leaf Area Index and branching level (primary to fourth level) and their spatial orientation were difficult to measure, hence literature values for MIMICS-I was used. The dielectric constant for crown and trunk layer components were evaluated by means of the empirical model developed by [41] due to difficulty in actual measurements. The soil moisture information was derived from the Wytham Woods test site during the AirSAR campaign, being collected by the Centre for Ecology and Hydrology on 23 June 2014. Different percentages of soil components for sand, silt and clay for all study sites were derived from the 1 km soil data set of Batjes [46].

There are sources of uncertainty related to calculating backscatter values from MIMICS-I model simulation. This is because the model simulation in this study has adopted published values for the number of leaves, needles and branch densities, branching level and their spatial orientation due to the difficulty in measuring these in the field. Secondly, the soil moisture information for all sites was derived from Wytham Woods during the AirSAR campaign which does not represent accurate moisture conditions of the forest stand, succession and open savanna. In addition, the MIMICS-I model works primarily for single even-aged or mono-species canopy which does not account for forest stands of mixed species composition, structure with multiple canopy layers and in degradation stages. Therefore, some uncertainty will be found in the model-derived backscatter due to the lack of actual ground information and model limitation.

Table 3. Input parameters for MIMICS-I model: normal = measured; italics = estimated.

	Parameter	Units	Broadleaved (17 Stands)	Needleleaved (8 Stands)
Trunk layer	Height	m	4, 3, 5, 3, 7, 8, 7, 8, 7, 10, 7, 6, 11, 12, 11, 8, 11	8, 10, 5, 10, 8, 12, 5, 7
	Diameter	m	1.7, 1.25, 1.26, 0.7, 1.6, 1.8, 2.6, 1.8, 1.5, 3.6, 2.6, 1.8, 3.3, 3.2, 2.2, 3.8, 2.3	1.9, 2.8, 0.8, 2.9, 1.8, 4.2, 1.2, 2.3
	Canopy density	m ⁻²	0.02, 0.02, 0.08, 0.35, 0.02, 0.02, 0.03, 0.02, 0.03, 0.02, 0.05, 0.18, 0.04, 0.04, 0.03, 0.02, 0.05	0.07, 0.07, 0.06, 0.06, 0.03, 0.04, 0.08, 0.03
	Moisture (gravimetric)	-	0.5	0.6
Crown layer	Crown thickness	m	5.2, 3, 6, 3.2, 7, 7.3, 8, 8.9, 6.9, 11.9, 8.3, 7.1, 12.5, 11.6, 11.4, 8.2, 10.9	11, 9.2, 5, 10.2, 7.3, 15, 5.4, 7.8
	Leaf/needle density	m ⁻³	830	100,000
	Leaf/needle moisture (gravimetric)	-	0.8	0.8
	Leaf Area Index (single-sided)	-	5	11.9
	Branch density (1st, 2nd, 3rd, 4th)	m ⁻³	4.1, 0.04, 0.45, 0.37	3.4
	Branch length (1st, 2nd, 3rd, 4th)	m	0.75, 1.15, 0.52, 0.33	2.0
	Branch diameter (1st, 2nd, 3rd, 4th)	cm	0.7, 1.6, 0.9, 0.57	2.0
	Branch Moisture	-	0.4	0.6
	Leaf/needle/branch orientation	-	Uniform	Uniform
	Dielectric constant (trunk, branch)	-	0.4	0.6
	Dielectric constant (leaf)	-	0.8	0.8
	Soil	Soil root mean square height	cm	0.45
Soil Correlation length		cm	18.75	18.75
Soil moisture (volumetric)		-	0.15	0.15
Sand		%	53	53
Silt		%	28	28
	Clay	%	19	19

2.4. SAR Data

An extensive S-band SAR campaign known as the “AirSAR Campaign”, was conducted in the UK in 2010 and 2014. The Airborne SAR Demonstrator Facility, ‘AirSAR’ is a collaborative project operated by Airbus Defence and Space (UK) with the Natural Environment Research Council (NERC) and the Satellite Applications Catapult. The S-band (3.1–3.3 GHz) has a swath width of 1.92 km and incidence angles from 16° to 42.5° with full polarimetry. The parameters of the AirSAR imageries acquired over Savernake Forest and Wytham Woods are summarised in Table 4. The Single-Look Complex (SLC) imagery is provided with 0.75 m pixel in both ground and cross-range spacing with 4.48 looks in azimuth and 1 look in range direction. Pre-processing of the amplitude image of the single look complex (SLC) S-band products of Savernake and Wytham study sites involves antenna pattern correction, slant to ground range and speckle filtered with the Enhanced Frost filter at 5 × 5 moving window. Details of SAR processing are given in Ningthoujam et al. [26]. Geo-coding of the SAR imagery is done using an ordnance map as a reference with 30 and 42 widely distributed ground control points (GCPs) for Savernake and Wytham sites using second-order polynomial and nearest neighbour re-sampling technique at 3.75 m pixel scale achieving RMSE of half a pixel. Finally, the images were re-sampled at 25 m pixel resolution to match the field sample size (Figure 1).

Table 4. Summary of the AirSAR data used in this study.

Site	Wytham Woods	Savernake Forest
Acquisition date	23 June 2014	24 June 2014
Day and Time (local time)	Monday, 12 h 15 m GMT	Tuesday, 15 h 39 m GMT
Aircraft altitude (m)	2407	3201
Look angles (°)	16–43.3	16–42.5
Image size (pixels)	26,633 (azimuth) × 1021 (range)	41,810 (azimuth) × 1298 (range)
Polarisation	HH, VV, HV, VH	HH, VV, HV, VH
Pixel spacing (m)	0.75	0.75

For the absolute radiometric calibration of airborne demonstrator data, imaging of the calibration target was achieved at near, centre and far locations of the full swath with corresponding incidence angles at 22.11°, 30.38° and 39.96° respectively. Conversion of the radar data to backscatter coefficient in dB was achieved using Equation (1) according to Airbus report [47]:

$$[\sigma^\circ = 10 \log_{10} (\text{DN}^2) - k_{\text{cal}}] \quad (1)$$

where: σ° = radar backscatter (dB), DN = digital number representing pixel intensity, and k_{cal} = calibration constant. The calibration constants for Savernake forest are: HH, VH = 71.8 dB; VV, HV = 72.62 dB and for Wytham Woods are: HH, VH = 81.46 dB and VV, HV = 81.9 dB.

3. Results and Discussion

3.1. S-Band Backscattering Simulation by MIMICS-I Model

By analysing scattering from each layer in the canopy, the backscattering from each polarisation was found to originate from different canopy components (Figure 2). At S-band, the total backscatter for the broadleaved canopy originates mainly from ground/trunk interactions at HH polarisation and from a combination of ground/trunk and volume scattering at VV polarisation. Direct crown scattering is the dominating scattering mechanism for cross-polarisation. This could be due to the reduced transmittance as a function of increasing leaf and branch density with HV polarisation signal [26]. The fourth level of branches produced strong backscatter for all polarisations particularly with HV polarisation in comparison to primary branches due to volume scattering from higher crown depth (leaves and branches). This shows that S-band backscatter can interact with different canopy components, particularly with branches, trunks and the ground layer depending on the canopy structure and polarisation. This modelling result supports the studies reported by Yatabe and Leckie [8] and Fransson et al. [9] who differentiated clear-cut stands against forest using Almaz S-band data. This modelling predicted S-band backscatter could also provide some information related to forest structure and biophysical parameters due to ground/trunk interactions as the dominant scattering.

For the Norway spruce canopy, the dominant scattering was from total crown due to high needle and branch density in comparison to broadleaved canopy. Alternatively, the high density of needles (100,000 m⁻³) and branches (3.4 m⁻³) used to model the canopy provides very low canopy transmissivities for all polarisations across the incidence angle range. Thus, a lower volume scattering is observed [15] possibly due to the randomised diffuse scattering from needles and small branches of conifers [26,48].

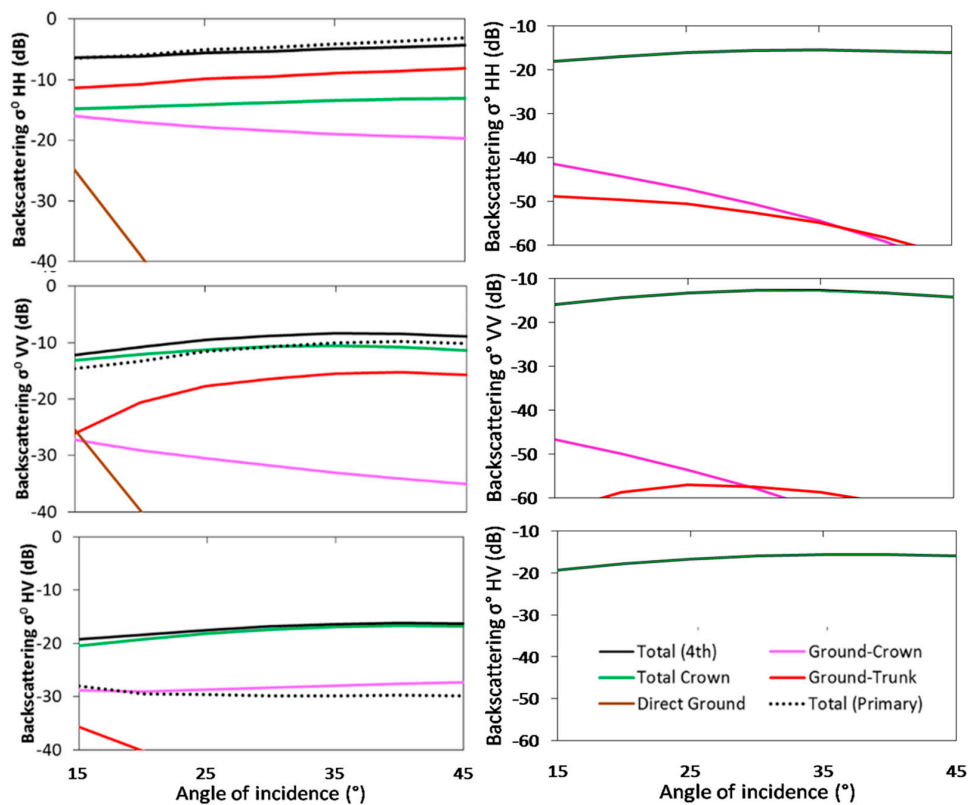


Figure 2. Total S-band co- and cross-polarised canopy backscatter components vs. scattering angle from 830 m^{-3} leaves *Betula pendula* at fourth and primary branch levels from 6 m height and 7 m crown thickness (**left**) and $10,000 \text{ m}^{-3}$ needle and 3.4 m^{-3} branch density from 8 m height 11 m crown thickness *Norway spruce* (**right**).

3.2. Comparison between MIMICS-I Simulations and SAR Data to Forest Aboveground Biomass

Relationships of observed and simulated S-band backscatter to plot-based forest aboveground biomass for Savernake and Wytham Woods within broadleaved and needleleaved stands are plotted in Figure 3. The co-polarised backscatter is highly dependent on forest AGB for broadleaved stands (Figure 3a, Table 5). For both observed and modeled S-band backscatter against forest AGB (broadleaved, needleleaved stands) the relationship follows a non-linear model where logarithmic model provides the best result. For model simulation, S-band backscatter increases with AGB giving an exponential rise to 100–120 t/ha at all polarisations, after which no further sensitivity is observed. This trend is more evident at VV and HV than at HH polarisation. For the airborne observations, S-band backscatter increases with AGB up to 150 t/ha at all polarisations. Furthermore, a good sensitivity of S-band SAR backscatter to forest AGB less than 100 t/ha in Savernake forest has been reported in a previous study [26], although the look angle can play a significant role in determining the overall backscatter as well.

Lower sensitivity of S-band backscatter to the forest biomass has been seen for needleleaved stands for the Savernake site for both model simulation and AirSAR (Figure 3b, Table 5). This could be due to the high density of foliage and branches in comparison to the broadleaved stand [41]. The mature conifers of the Savernake forest have high biomass content and the S-band backscatter signal is saturated at these high biomass levels. The observed discrepancies between measured and simulated backscatter can be attributed to errors associated to field data, AirSAR calibration and modelling resulting to over/under-estimation of the canopy volume scattering. Detailed information is given in Section 3.4.

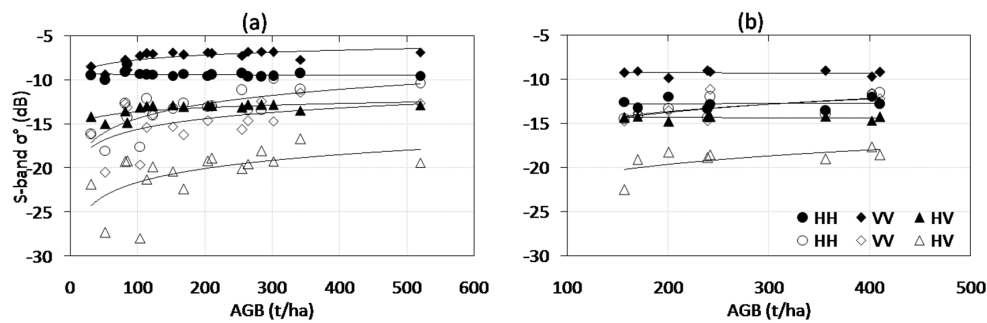


Figure 3. Observed (no fill) against Simulated (filled) backscatter for S-band as a function of varying forest AGB for (a) broadleaved and (b) needleleaved stands at different polarisations at 30° incidence angle. Best fit log relationships were fitted for (a,b).

Table 5. Results of biomass regression models using S-band backscatter. r^2 is the coefficient of determination and RMSE is the root mean square error (t/ha) calculated using 17 broadleaved and 8 needleleaved plots.

Polarisation	AirSAR				MIMICS-I			
	Broadleaved		Needleleaved		Broadleaved		Needleleaved	
	r^2	RMSE (t/ha)	r^2	RMSE (t/ha)	r^2	RMSE (t/ha)	r^2	RMSE (t/ha)
HH	0.58	1.50 **	0.47	0.96 *	0.01	0.38 ns	0.00	0.63 ns
VV	0.27	2.12 *	0.32	1.21 ns	0.52	0.56 **	0.00	0.34 ns
HV	0.31	2.53 *	0.36	1.25 ns	0.48	0.52 **	0.00	0.23 ns

p-Value: ** <0.005, * <0.05, ns—not significant.

3.3. MIMICS-I Simulated S-Band Backscatter against Forest Biomass

3.3.1. Broadleaved Forest Stand

Relationships of simulated S-band backscatter and plot-based forest aboveground biomass for broadleaved stands are plotted in Figure 4. S-band backscatter is dependent on forest AGB and shows varying sensitivity at different polarisations for different sites. The modeled S-band backscatter against forest AGB shows a logarithmic model as the best relationship for broadleaved stand. S-band backscatter increases with AGB giving an exponential rise to around 100–120 t/ha at all polarisations, after which no further sensitivity is observed. This trend is more evident at VV and HV than at HH polarisation. VV backscatter increases by over 3 dB as AGB increases from low AGB (secondary forest, savanna forest, etc.) up to 300 t/ha. VV polarised backscatter produces the highest sensitivity to AGB with $r^2 = 0.84$ (RMSE = 0.28 t/ha, $p < 0.0001$) for the Tapajós site, except for the Himalaya broadleaved forest site (Table 6). The high sensitivity of S-band backscatter to AGB at the Tapajós site could be due to the lower 8 t/ha biomass for secondary succession stages to 271.82 t/ha biomass for intact primary forest. Similar levels of P-band backscatter sensitivity to forest AGB up to ≤ 100 t/ha at HH and HV polarisations at Tapajós has been observed by Santos, et al. [7]. L-band backscatter from PALSAR shows sensitivity to forest AGB up to ≤ 100 t/ha for HH polarisation at the forest-savanna boundary in Cameroon by Mitchard et al. [6].

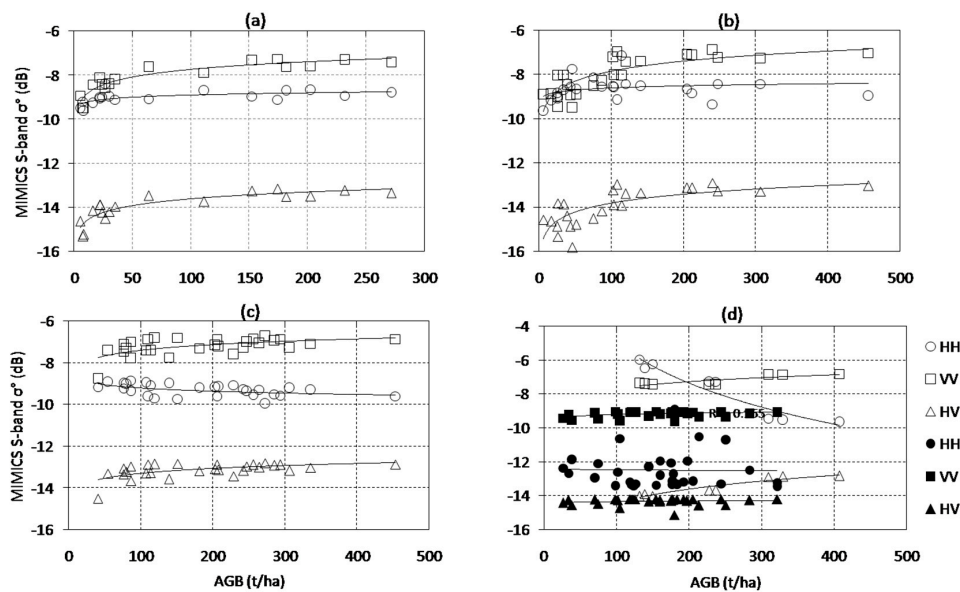


Figure 4. Simulated backscatter for S-band against forest AGB as a function of varying forest biomass for Tapajós (a); Cameroon (b); Dudhwa National Park (c); and Kashmir (d) for broadleaved (no fill) and needleleaved (filled) stands at different polarisations at 30° incidence angle. Best fit log relationships were fitted for (a–d).

Table 6. Results from the regression models relating MIMICS-I simulated S-band backscatter (σ°) to plot biomass for broadleaved stands. r^2 is the coefficient of determination and RMSE is the root mean square error (t/ha) calculated using plots.

Site	Polarisation	r^2	RMSE (t/ha)	Slope Confidence Interval	
				Lower 95%	Upper 95%
Tapajós	HH	0.39	0.23 *	−9.94	−9.17
	VV	0.84	0.28 ***	−10.51	−9.57
	HV	0.79	0.3 ***	−16.17	−15.18
Cameroon	HH	0.07	0.5 ns	−10.18	−8.3
	VV	0.63	0.52 ***	−11.81	−9.88
	HV	0.53	0.57 ***	−17.55	−15.41
Himalaya	HH	0.91	0.49 **	16.99	5.47
	VV	0.66	0.18 *	−12.52	−8.11
	HV	0.88	0.19 **	−22.04	−17.47
Dudhwa	HH	0.22	0.25 **	−9.02	−7.33
	VV	0.33	0.35 **	−10.38	−8.06
	HV	0.34	0.28 **	−15.82	−13.91

p-Value: *** <0.0001, ** <0.005, * <0.05, ns—not significant.

HV-polarised backscatter shows the greatest sensitivity to AGB with $r^2 = 0.88$ (RMSE = 1.9 t/ha, $p < 0.0001$) for the Himalaya and Tapajós study sites and medium sensitivity for the Cameroon site. Similar ranges of backscatter with 3 dB are observed at HV polarisation for the AGB range. Finally, the HH-polarised backscatter has the lowest sensitivity to AGB with $r^2 = 0.39$ (RMSE = 0.23 t/ha, $p < 0.00001$) (Table 6). P-band HV backscatter sensitivity to forest AGB up to 100 t/ha at the Tapajós site has also been reported by Santos et al. [7]. A slightly greater sensitivity of L-band HV backscatter to 150 t/ha AGB has been observed at the forest-savanna boundary in Cameroon by Mitchard et al. [6]. When all the plots were combined, a lower sensitivity of all polarisations to AGB was observed with strongest sensitivity at VV- and HV-polarised backscatter with $r^2 = 0.66$ (RMSE = 0.44 t/ha, $p < 0.0001$) and 0.58 (RMSE = 0.46 t/ha, $p < 0.0001$).

Using the logarithmic model from the above relationship between simulated S-band backscatter and forest AGB, the AGB for broadleaved forests for all sites are predicted (Table 7). The lowest RMSE for the Tapajós site was 44 t/ha at VV and for the Himalaya site, 33.8 t/ha at HH-polarised. Comparing the r^2 and RMSE of AGB retrieved from all polarisations, S-band co-polarised backscatter at VV-polarization is generally better suited for biomass retrieval than the cross-polarised backscatter, with higher accuracies similar to [26].

Table 7. Results of biomass regression models using MIMICS-I simulated S-band backscatter. r^2 is the coefficient of determination and RMSE is the root mean square error (t/ha) calculated using plots.

Polarisation	Savernake/WW		Tapajós		Cameroon		Himalaya		Dudhwa	
	r^2	RMSE	r^2	RMSE	r^2	RMSE	r^2	RMSE	r^2	RMSE
HH	0.1	122.53 ns	0.00	92.24 ns	0.00	112.51 ns	0.9	33.8 **	0.34	155.92 *
VV	0.32	106.48 *	0.76	44.74 ***	0.59	71.39 ***	0.78	50.43 **	0.58	125.17 *
HV	0.31	107.04 *	0.71	48.99 ***	0.57	73.37 ***	0.87	37.88 **	0.34	155.86 *

p-Value: *** < 0.0001, ** < 0.005, * < 0.05, ns—not significant.

3.3.2. Needleleaved Forest Stand

The modeled S-band backscatter against forest AGB shows a logarithmic model as the best result for conifer stands. The relationship of S-band polarimetry against plot AGB for needleleaved stands (Figure 4d) shows that both co- and cross-polarised backscatter are only weakly related to AGB showing less sensitivity to forest biomass at stand level for the Himalaya site (Table 8). The poor relationship of S-band backscatter to forest biomass for needleleaved stands could possibly be due to the randomized diffuse scattering from the high density of needle foliage and branches in comparison to the broadleaved stand [41,42,48]. S-band microwave pulses do not penetrate deeply enough into the forest canopy in the mature conifer stands at the Himalayan site, irrespective of their AGB.

Table 8. Results from the regression models relating MIMICS-I simulated S-band backscatter (σ^0) to plot biomass for conifer stands in the Himalayas. r^2 is the coefficient of determination and RMSE is the root mean square error (t/ha) calculated using plots.

Polarisation	r^2	RMSE	Slope Confidence Interval	
			Lower 95%	Upper 95%
HH	0.0	1.09 ns	−15.66	−9.05
VV	0.16	0.16 *	−10.23	−9.25
HV	0.01	0.2 ns	−15.15	−13.9

p-Value: * < 0.05, ns—not significant.

A consensus is that backscatter increases only for relatively low biomass ranges and the signal saturates at higher biomass. Results supporting this have been reported for different radar wavelengths, particularly at L-band and no saturation at P-band [6,7]. At S-band, VV and HV polarisations were found to be useful for forest structural retrieval for broadleaved species because of a strong ground/trunk interaction contribution to the backscatter. However, a weak relationship is found between S-band radar backscatter and needleleaved biomass, possibly due to the thick density of needles and branches, resulting in random scattering from the canopy.

Simulated S-band backscatter-biomass relationships suggest increasing backscatter sensitivity to forest AGB with a saturation level ≤ 100 t/ha and the smallest achievable error between 37 t/ha and 44 t/ha and r^2 between 0.31 and 0.9 for HV and VV polarisations in the low to medium incidence angle range. This is consistent with previous study where the relationship of S-band backscatter with forest stands up to 300 t/ha biomass has shown the best achievable error between 90.63 and 99.39 t/ha in the temperate mixed forest of Savernake Forest [26].

3.4. Model Accuracy

The observed discrepancies between measured and simulated backscatter can be attributed to four main factors, as discussed below. Firstly, any inaccuracies in field data collection (e.g., diameter, height and crown depth) and biophysical derivations have resulted in estimation error of the model as the model is sensitive to the dimensions, density and dielectric constant of the canopy components. Secondly, the lack of soil moisture information for all sites except for Wytham Woods introduces uncertainty due to the sensitivity of the SAR signal to moisture content (dielectric). Thirdly, the model simulation does not include the multiple scattering mechanism among canopy elements and did not account for mixed-species composition with varying canopy layers due to the limitation of the first-order radiative transfer model [44]. The above three factors could collectively produce over/under-estimation of the total canopy scattering from the forest stand. Finally, errors are also associated with the acquisition of AirSAR data and subsequent calibration accuracy.

4. Conclusions

This study combined radiative transfer model simulations from MIMICS-I with an analysis of experimental AirSAR S-band backscatter data to understand the scattering mechanisms from forest canopies. The results suggest a greater sensitivity of the S-band backscatter signal to forest AGB for broadleaved species up to 100 t/ha. Moreover, simulated S-band backscatter suggests that S-band SAR may be able to provide information on forest biomass in low-biomass forests up to 100 t/ha with the smallest achievable errors between 37 t/ha and 44 t/ha for HV and VV polarisations in different forest types, particularly broadleaved forest in temperate and tropical forest.

Current (Huan Jing-1 Constellation) and future (NovaSAR-S and NISAR) space-borne S-band SAR missions will continue to provide opportunities to monitor forest properties. This study highlighted that S-band SAR data from these sensors are likely to be suitable for deriving forest structural information, particularly aboveground woody biomass for temperate mixed forests, secondary forests and savanna woodlands of the tropics. Comparison of the model simulated against observed backscatter at S-band for relating to forest structure information at these sites might be investigated in future when data is available. This includes observation data from NovaSAR and NISAR data against biomass of tree components (branch biomass, stem biomass, total biomass) to infer better levels of the saturation point. Therefore, in the future, the challenge will be the full integration of SAR data from currently available L-band 'ALOS-2 PALSAR-2' and future P-band 'BIOMASS mission', and the S-band missions 'NovaSAR-S' and 'NISAR' which have high potential for a better quantification of forest biomass at regional to global scales.

Acknowledgments: The authors acknowledge Leland Pierce from the Radiation Lab, The University of Michigan (United States of America) for providing the MIMICS-I code. MIMICS simulation was performed using ALICE High Performance Computing Facility at the University of Leicester. The AirSAR 2014 data was procured from Airbus Defence and Space, Satellite Applications Catapult and Natural Environment Research Council Airborne Research & Survey Facility. We thank João R. Santos (INPE, Brazil) for providing their published field data table. We also thanked Yadvinder Malhi (SOGE, University of Oxford), Jon Lloyd (Life Sciences, Imperial College University), Simon L. Lewis (Geography, University College London and University of Leeds), Bonaventure Sonké (Biology, University of Yaoundé), Keith Morrison (University of Reading), France Gerard, Charles George (Centre for Ecology and Hydrology), Geoff Burbidge, Sam Doody, Van Beijma Sybrand (Airbus Defence and Space), Nick Veck (Satellite Applications Catapult), Gary M. Llewellyn (Natural Environment Research Council Airborne Research & Survey Facility), Thomas Blythe (Forestry Commission, Bristol and Saverlake), Sarah C.M. Johnson, Pedro Rodriguez-Veiga, Bernard Spies, James E.M. Wheeler, Chloe Barnes, Valentin Louis, Tom Potter, Marc Padilla, Alexander Edwards-Smith and Jaime Polo Bermejo for their invaluable contributions. The Environmental Change Network plot database for Wytham Woods being shared by Lorna Sherrin from Centre for Ecology & Hydrology (CEH) is also appreciated. Heiko Balzter was supported by the Royal Society Wolfson Research Merit Award, 2011/R3 and the NERC National Centre for Earth Observation. Pawan K. Joshi is thankful to DST-PURSE of Jawaharlal Nehru University for research support. We would like to thank all three reviewers and academic editors for their comments, which has helped us to improve the quality of our manuscript.

Author Contributions: This research study was designed and developed by Ramesh K. Ningthoujam, Heiko Balzter and Kevin Tansey in support to NovaSAR future mission for forestry applications. Ramesh K. Ningthoujam processed, simulated and analysed AirSAR and MIMICS-I model predictions (assisted

by Kevin Tansey and Heiko Balzter), wrote the manuscript and coordinated revisions. Edward T.A. Mitchard, Akhlaq A. Wani and Pawan K. Joshi provided the field plot data from Cameroon, Kashmir and DNP. All authors commented on the analysis and contributing substantially to revisions.

Conflicts of Interest: The authors declare no conflict of interest.

Appendix A

Table A1. Measured input parameters from Tapajós, Cameroon, Kashmir and Dudhwa National Park (DNP) forest plots for MIMICS-I model simulation.

Tapajós	Parameter	Units	Primary Forest (6)	Secondary Forest (12)
Trunk layer	Height	m	6, 5, 5, 6, 6, 6	5, 4.4, 3.1, 3, 5, 5, 4, 4, 4, 2.5, 2, 2
	Diameter	m	1.4, 1.2, 1.2, 1.3, 1.3, 1.5	1.2, 0.9, 0.6, 0.5, 0.8, 0.7, 0.6, 0.7, 0.8, 0.5, 0.5, 0.3
	Canopy density	m ⁻²	0.29, 0.3, 0.28, 0.23, 0.27, 0.17	0.24, 0.11, 0.15, 0.31, 0.11, 0.16, 0.14, 0.26, 0.08, 0.07, 0.09, 0.17
Crown layer	Crown thickness	m	6, 6.2, 6.2, 6.5, 6.7, 7	5.3, 5, 4, 3.7, 4.7, 4.2, 3.9, 3.9, 3.3, 3, 2.8, 1.7
Soil	Sand	%		44
	Silt	%		26
	Clay	%		30
Cameroon	Parameter	Units	Broadleaved (24)	
Trunk layer	Height	m	3, 3, 3, 4, 3, 4, 3, 3, 3, 3, 3, 3, 3, 6, 4, 7, 4, 6, 6, 7, 7, 8, 6, 8, 7	
	Diameter	m	1.1, 1.7, 1.6, 2, 1.2, 1.8, 1.8, 1.1, 1.1, 1.5, 1.5, 1.7, 1.2, 1.4, 2, 1.2, 1.4, 1.2, 1.4, 2, 2.1, 1.3, 2.3, 2.4	
	Canopy density	m ⁻²	0.04, 0.13, 0.21, 0.1, 0.2, 0.24, 0.31, 0.27, 0.45, 0.24, 0.39, 0.28, 0.57, 0.27, 0.46, 0.79, 0.51, 0.47, 0.64, 0.46, 0.46, 0.64, 0.61, 0.51	
Crown layer	Crown thickness	m	3.6, 3.5, 3.2, 4.1, 2.7, 4, 3.9, 3.2, 2.3, 3.3, 3.7, 4.3, 6.8, 4.9, 8.4, 5.1, 5.8, 6, 6.6, 6.6, 8.8, 6.5, 9.4, 7.6	
Soil	Sand	%	48	
	Silt	%	22	
	Clay	%	30	
Kashmir	Parameter	Units	Broadleaved (8)	Needleleaved (31)
Trunk layer	Height	m	5, 5, 10, 10, 10, 4, 4, 4	10, 10, 8, 10, 10, 10, 6, 8, 8, 4, 5, 11, 4, 12, 13, 15, 12, 13, 7.8, 13, 12, 10, 8, 7, 6, 8, 7, 6, 7, 10, 5
	Diameter	m	1.4, 1.4, 3.8, 3.5, 3.8, 1.2, 1.3, 1.3	6.2, 5.4, 4.1, 6.1, 5.9, 5.6, 2.6, 3.7, 2.8, 1.5, 1.8, 6.3, 2, 5.8, 7.6, 12, 7.6, 6.1, 4.7, 6.5, 5.6, 8, 4.6, 6, 2.3, 2.9, 1.9, 2.1, 2.2, 5.3, 1.9
	Canopy density	m ⁻²	1.13, 1.15, 0.34, 0.38, 0.34, 2.19, 1.7, 1.8	0.13, 0.16, 0.3, 0.12, 0.15, 0.18, 0.16, 0.1, 0.45, 0.9, 0.8, 0.09, 0.52, 0.25, 0.04, 0.06, 0.1, 0.1, 0.1, 0.1, 0.1, 0.1, 0.12, 0.03, 0.6, 0.2, 0.79, 0.77, 0.26, 0.09, 0.76
Crown layer	Crown thickness	m	5.7, 5.7, 14.5, 12.3, 13, 3.9, 4.2, 3.9	12.7, 10, 8.3, 12, 11.9, 9.5, 6, 7.3, 7.7, 5, 6, 13, 4.2, 12.3, 14.7, 14.2, 13.2, 14.3, 10, 13, 13.2, 12.6, 8.6, 10, 7.4, 8.3, 7, 7.7, 7.6, 13.2, 6.1
Soil	Sand	%	44	
	Silt	%	37	
	Clay	%	19	
DNP	Parameter	Units	Broadleaved (28)	
Trunk layer	Height	m	3, 7, 8, 6, 7, 7, 4, 7, 10, 6, 10, 5, 10, 6, 7, 9, 8, 6, 6, 7, 9, 7, 14, 9, 9, 7, 8, 9	
	Diameter	m	1.9, 2.1, 2.5, 2.5, 1.8, 2.5, 2, 2.4, 3.5, 2.5, 3.3, 1.9, 3.9, 2.4, 2.6, 3.5, 2.9, 2.4, 2.6, 3.1, 2.6, 2.6, 2.6, 4.1, 2.7, 3, 2.2, 3.8	
	Canopy density	m ⁻²	0.13, 0.2, 0.16, 0.18, 0.2, 0.18, 0.2, 0.21, 0.08, 0.12, 0.1, 0.14, 0.08, 0.09, 0.17, 0.1, 0.17, 0.12, 0.06, 0.14, 0.14, 0.17, 0.12, 0.1, 0.15, 0.1, 0.13, 0.12	
Crown layer	Crown thickness	m	3.6, 7.1, 11, 7.9, 7.7, 10.6, 5.6, 7.2, 10, 7.3, 11.2, 5.9, 11.7, 7, 8.8, 11.9, 10.4, 6.4, 7, 10.4, 10.5, 9.7, 16.6, 9.5, 10.7, 8, 8.6, 10.9	
Soil	Sand	%	45	
	Silt	%	33	
	Clay	%	22	

References

1. Saatchi, S.S.; Harris, N.L.; Brown, S.; Lefsky, M.; Mitchard, E.T.; Salas, W.; Zutta, B.R.; Buermann, W.; Lewis, S.L.; Hagen, S.; et al. Benchmark map of forest carbon stocks in tropical regions across three continents. *Proc. Natl. Acad. Sci. USA* **2011**, *108*, 9899–9904. [[CrossRef](#)] [[PubMed](#)]
2. Mitchard, E.T.A.; Feldpausch, T.R.; Brienen, R.J.W.; Lopez-Gonzalez, G.; Monteagudo, A.; Baker, T.R.; Lewis, S.L.; Lloyd, J.; Quesada, C.A.; Gloor, M.; et al. Markedly divergent estimates of Amazon forest carbon density from ground plots and satellites. *Glob. Ecol. Biogeogr.* **2014**, *23*, 935–946. [[CrossRef](#)] [[PubMed](#)]
3. Woodhouse, I.H.; Mitchard, E.T.A.; Brolly, M.; Maniatis, D.; Ryan, C.M. Radar backscatter is not a ‘direct measure’ of forest biomass. *Nat. Clim. Chang.* **2012**, *2*, 556–557. [[CrossRef](#)]
4. Clark, D.B.; Kellner, J.R. Tropical forest biomass estimation and the fallacy of misplaced concreteness. *J. Veg. Sci.* **2012**, *23*, 1191–1196. [[CrossRef](#)]
5. Lucas, R.M.; Armston, J.; Fairfax, R.; Fensham, R.; Accad, A.; Carreiras, J.; Kelley, J.; Bunting, P.; Clewley, D.; Bray, S.; et al. An evaluation of the ALOS PALSAR L-band backscatter—Above ground biomass relationship Queensland, Australia: Impacts of surface moisture condition and vegetation structure. *IEEE J. Sel. Top. Appl. Earth Obs. Remote Sens.* **2010**, *3*, 576–593. [[CrossRef](#)]
6. Mitchard, E.T.A.; Saatchi, S.S.; Lewis, S.L.; Feldpausch, T.R.; Woodhouse, I.H.; Sonké, B.; Rowland, C.; Meir, P. Measuring biomass changes due to woody encroachment and deforestation/degradation in a forest–savanna boundary region of Central Africa using multi-temporal L-band radar backscatter. *Remote Sens. Environ.* **2011**, *115*, 2861–2873. [[CrossRef](#)]
7. Santos, J.R.; Freitas, C.C.; Araujo, L.S.; Dutra, L.V.; Mura, J.C.; Gama, F.F.; Soler, L.S.; Sant’Anna, S.J.S. Airborne P-band SAR applied to the aboveground biomass studies in the Brazilian tropical rainforest. *Remote Sens. Environ.* **2003**, *87*, 482–493. [[CrossRef](#)]
8. Yatabe, S.M.; Leckie, D.G. Clearcut and forest-type discrimination in satellite SAR imagery. *Can. J. Remote Sens.* **1995**, *21*, 455–467. [[CrossRef](#)]
9. Fransson, J.E.S.; Walter, F.; Olsson, H. Identification of clear felled areas using Spot P and Almaz-1 SAR data. *Int. J. Remote Sens.* **1999**, *20*, 3583–3593. [[CrossRef](#)]
10. Rosenqvist, Å. Evaluation of JERS-1, ERS-1 and Almaz SAR backscatter for rubber and oil palm stands in West Malaysia. *Int. J. Remote Sens.* **1996**, *17*, 3219–3231. [[CrossRef](#)]
11. Olsson, H.; Naslund, B.; Hagner, O.; Sylvander, R. Early experience on the use of satellite borne S-band sar over Swedish forests. In *Workshop on Remote Sensing for Forestry Applications*; Report EUR 14445 EN; Commission of the European Communities JRC ISPRA: Copenhagen, Denmark, 1991; pp. 223–230.
12. Brown, R.J.; Brisco, B.; Ahern, F.; Yatabe, S.M.; Drieman, J. Preliminary ERS-1 assessment for Canadian agriculture and forestry applications. In *Proceedings of the First ERS-1 Symposium, Cannes, France, 4–6 November 1992*; pp. 611–616.
13. Lopez-Sanchez, J.M.; Ballester-Berman, J.D.; Fortuny-Guasch, J. Indoor wide-band polarimetric measurements on maize plants a study of the differential extinction. *IEEE Trans. Geosci. Remote Sens.* **2006**, *44*, 758–767. [[CrossRef](#)]
14. Sun, Q.; Zhang, F.; Shao, Y.; Liu, L.; Wang, G.; Bian, Z.; Li, K. S-band backscattering analysis of wheat using tower-based scatterometer. In *Proceedings of the 2012 IEEE International Geoscience and Remote Sensing Symposium, Munich, Germany, 22–27 July 2012*; pp. 4621–4624.
15. Lopez-Sanchez, J.M.; Fortuny-Guasch, J.; Cloude, S.R.; Sieber, A.J. Indoor polarimetric radar measurements on vegetation samples at L, S, C and X band. *J. Electromagn. Waves Appl.* **2000**, *14*, 205–231. [[CrossRef](#)]
16. Guida, R.; Natale, A.; Bird, R.; Whittaker, P.; Cohen, M.; Hall, D. Canopy classification with S-band polarimetric SAR data. In *Proceedings of the 2012 IEEE International Geoscience and Remote Sensing Symposium, Munich, Germany, 22–27 July 2012*; pp. 6535–6538.
17. Natale, A.; Guida, R.; Bird, R.; Whittaker, P.; Hall, D.; Cohen, M. Validation of S-band data performance for future space borne SAR missions. In *Proceedings of the 9th European Conference on Synthetic Aperture Radar, Nurnberg, Germany, 24 April 2012*; pp. 75–78.
18. Van Beijma, S.; Comber, A.; Lamb, A. Random forest classification of salt marsh vegetation habitats using quad-polarimetric airborne SAR, elevation and optical RS data. *Remote Sens. Environ.* **2014**, *149*, 118–129. [[CrossRef](#)]

19. Woodhouse, I.H. Predicting backscatter-biomass and height-biomass trends using a macroecology model. *IEEE Trans. Geosci. Remote Sens.* **2006**, *44*, 871–877. [[CrossRef](#)]
20. Fransson, J.E.S.; Israelsson, H. Estimation of stem volume in boreal forests using ERS-1 C- and JERS-1 L-band SAR data. *Int. J. Remote Sens.* **1999**, *20*, 123–137. [[CrossRef](#)]
21. Brolly, M.; Woodhouse, I.H. Vertical backscatter profile of forests predicted by a macroecological plant model. *Int. J. Remote Sens.* **2013**, *34*, 1026–1040. [[CrossRef](#)]
22. Smith-Jonforsen, G.; Folkesson, K.; Hallberg, B.; Ulander, L.M.H. Effects of forest biomass and stand consolidation on P-band backscatter. *IEEE Geosci. Remote Sens. Lett.* **2007**, *4*, 669–673. [[CrossRef](#)]
23. Le Toan, T.; Beaudoin, A.; Riom, J.; Guyon, D. Relating forest biomass to SAR data. *IEEE Trans. Geosci. Remote Sens.* **1992**, *30*, 403–411. [[CrossRef](#)]
24. Baker, J.R.; Mitchell, P.L.; Cordey, R.A.; Groom, G.B.; Settle, J.J.; Stileman, M.R. Relationships between physical characteristics and polarimetric radar backscatter for Corsican pine stands in Thetford Forest, U.K. *Int. J. Remote Sens.* **1994**, *15*, 2827–2849. [[CrossRef](#)]
25. Le Toan, T.; Quegan, S.; Davidson, M.W.J.; Balzter, H.; Paillou, P.; Papathanassiou, K.; Plummer, S.; Rocca, F.; Saatchi, S.; Shugart, H.; et al. The BIOMASS mission: Mapping global forest biomass to better understand the terrestrial carbon cycle. *Remote Sens. Environ.* **2011**, *115*, 2850–2860. [[CrossRef](#)]
26. Ningthoujam, R.K.; Balzter, H.; Tansey, K.; Morrison, K.; Johnson, S.C.M.; Gerard, F.; George, C.; Malhi, Y.; Burbidge, G.; Doody, S.; et al. Airborne S-band SAR for forest biophysical retrieval in temperate mixed forests of the UK. *Remote Sens.* **2016**, *8*, 609. [[CrossRef](#)]
27. Crutchley, S.P.; Small, F.; Bowden, M. *Savernake Forest: A Report for the National Mapping Programme*; English Heritage: Swindon, UK, 2009; pp. 1–75.
28. Hall, J.E.; Kirby, K.J.; Whitbread, A.M. *National Vegetation Classification: Field Guide to Woodland*; Joint Nature Conservation Committee: Peterborough, UK, 2004.
29. Radambrasil, P. *Folha SA. 21 Santarém; Geologia, Geomorfologia, Solos, Vegetação e uso Potencial da Terra*; Levantamento de Recursos Naturais, 10: Rio de Janeiro, Brazil, 1976; 522p.
30. Doumenge, C.; Ndinga, A.; Nembot, T.F.; Tchanou, Z.; Ondo, V.M.; Nze, N.O.; Bourobou, B.H.P.; Ngoye, A. Forest biodiversity conservation in atlantic regions of Central Africa: ii. Identifying a network of critical sites. *Bois For. Trop.* **2003**, *296*, 43–58.
31. Feldpausch, T.R.; Banin, L.; Phillips, O.L.; Baker, T.R.; Lewis, S.L.; Quesada, C.A.; Affum-Baffoe, K.; Arets, E.J.M.M.; Berry, N.J.; Bird, M.; et al. Height-diameter allometry of tropical forest trees. *Biogeosciences* **2011**, *8*, 1081–1106. [[CrossRef](#)]
32. Champion, H.G.; Seth, S.K. *A Revised Survey of Forest Types of India*; New Delhi Government Publication: New Delhi, India, 1968.
33. Environmental Change Network; Centre for Ecology and Hydrology. Data Citation Code: Ecn:Rn12/14. Available online: <http://data.ecn.ac.uk> (accessed on 22 January 2015).
34. Wani, A.A. Integrated Resource Assessment of Forest Carbon Stock in Himalayan Region of South Kashmir. Ph.D. Thesis, Forestry (Forest Management), Forest Research Institute, Deemed University, Dehradun, India, 2013.
35. Ningthoujam, R.K. Forest Cover, Stand Volume and Biomass Assessment in Dudhwa National Park Using Satellite Remote Sensing Data (Optical and Envisat ASAR). Master's Thesis, Andhra University, Visakhapatnam, India, 2007. Available online: www.iirs.gov.in/iirs/sites/default/files/StudentThesis/biomass_assessment_asar_ramesh.pdf (accessed on 31 October 2007).
36. Zianis, D.; Muukkonen, P.; Mäkipää, R.; Mencuccini, M. Biomass and stem volume equations for tree species in Europe. *Silva Fenn. Monogr.* **2005**, *4*, 4–63.
37. Brown, S.; Gillespie, A.J.R.; Lugo, A.E. Biomass estimation methods for tropical forest with applications to forest inventory data. *For. Sci.* **1989**, *35*, 881–902.
38. Uhl, C.; Buschbacher, R.; Serrão, E.A.S. Abandoned pastures in eastern amazonia: I. Patterns of plant succession. *J. Ecol.* **1988**, *76*, 663–681. [[CrossRef](#)]
39. Chave, J.; Andalo, C.; Brown, S.; Cairns, M.A.; Chambers, J.Q.; Eamus, D.; Fölster, H.; Fromard, F.; Higuchi, N.; Kira, T.; et al. Tree allometry and improved estimation of carbon stocks and balance in tropical forests. *Oecologia* **2005**, *145*, 87–99. [[CrossRef](#)] [[PubMed](#)]
40. Forest Survey of India. *Volume Equations for Forests of India, Nepal, and Bhutan*; Forest Survey of India, Ministry of Environment & Forests, Government of India: India, 1996; p. 249.

41. Ulaby, F.T.; Sarabandi, K.; McDonald, K.; Whitt, M.; Dobson, M.C. Michigan microwave canopy scattering model. *Int. J. Remote Sens.* **1990**, *11*, 1223–1253. [[CrossRef](#)]
42. Bosisio, A.V.; Dechambre, M. Predictions of microwave attenuation through vegetation: A comparison with measurements. *Int. J. Remote Sens.* **2004**, *25*, 3973–3997. [[CrossRef](#)]
43. Karam, M.A.; Amar, F.; Fung, A.K.; Mougou, E.; Lopes, A.; Le Vine, D.M.; Beaudoin, A. A microwave polarimetric scattering model for forest canopies based on vector radiative transfer theory. *Remote Sens. Environ.* **1995**, *53*, 16–30. [[CrossRef](#)]
44. Liang, P.; Moghaddam, M.; Pierce, L.E.; Lucas, R.M. Radar backscattering model for multilayer mixed-species forests. *IEEE Trans. Geosci. Remote Sens.* **2005**, *43*, 2612–2626. [[CrossRef](#)]
45. Grover, K.; Quegan, S.; Freitas, C.D. Quantitative estimation of tropical forest cover by SAR. *IEEE Trans. Geosci. Remote Sens.* **1999**, *37*, 479–490. [[CrossRef](#)]
46. Batjes, N.H. *World Soil Property Estimates for Broad-Scale Modelling (Wise30sec)*; Report 2015/01; Isric—World Soil Information: Wageningen, The Netherlands, 2015.
47. Airbus. *Airborne SAR Demonstrator Facility (Airsar) d2: User Guide*; Airbus Defence and Space: Hampshire, UK, 2013; pp. 1–43.
48. Morrison, K.; Bennett, J.; Solberg, S. Ground-based C-band tomographic profiling of a conifer forest stand. *Int. J. Remote Sens.* **2013**, *34*, 7838–7853. [[CrossRef](#)]



© 2017 by the authors. Licensee MDPI, Basel, Switzerland. This article is an open access article distributed under the terms and conditions of the Creative Commons Attribution (CC BY) license (<http://creativecommons.org/licenses/by/4.0/>).